JOURNAL OF MATERIALS SCIENCE 29 (1994) 1739–1752

Effect of glass-fibre reinforcement and annealing on microstructure and mechanical behaviour of nylon 6,6

Part II *Mechanical behaviour*

M. L. SHIAO, S. V. NAIR
Department of Mechanical Engineering, University of Massachusetts, Amherst, MA 01003, USA

P. D. GARRETT, R. E. POLLARD
Monsanto Chemical Co., Springfield, MA 01151, USA

The effects of glass-fibre reinforcement and annealing on the deformation and fracture behaviour of nylon 6,6 were investigated. The roles of glass fibres were examined by varying the glass fibre content and the fibre length, and by *in situ* fracture studies in front of crack tips. The effects of microstructural changes were investigated by imposing various annealing conditions on the specimens. The results indicated that the fracture toughness showed a sharp decrease due to stress concentrations at fibre ends when the fibre volume fraction was small. Above a critical fibre volume fraction, it was found that the fracture toughness can be substantially increased by enhanced localized matrix plasticity at fibre ends. The competing roles of glass fibre ends were consistent with microstructure sensitive fracture mechanics models of failure based on the attainment of a critical stress or strain over a critical microstructural distance in the crack-tip region. Upon annealing above a critical annealing time the unreinforced nylon 6,6 showed a drastic decrease in the strength and ductility, corresponding to a loss of the constant-load deformation region prior to necking. However, the fracture toughness of unreinforced nylon 6,6 was only moderately reduced by annealing. On the other hand, the fracture toughness of the composites showed a significant increase upon annealing. The combined effects of glass fibres and annealing on microstructures and overall property optimization of the composites are also discussed.

1. Introduction

Short glass fibre-reinforced semi-crystalline polymers, such as glass fibre-reinforced nylon 6,6, have been increasingly used in many structural applications owing to their enhanced mechanical properties [1–5]. It is known that the glass fibres can increase the material's strength and modulus, but can also decrease the material's ductility significantly, and thereby limit the property enhancement [6]. For example, in glass fibre-reinforced nylon 6,6, the tensile modulus of nylon 6,6 was substantially improved by glass fibres; however, the strength enhancement was limited by an embrittlement effect at fibre ends [7]. Tensile failure of such composites occurred by the initiation and propagation of interfacial cracks formed at fibre ends [7–9]. On the other hand, upon loading, significant localized plastic deformation around the glass fibres was also observed in the composites [7, 10]. As the amount of glass fibre increases, such localized matrix plasticity can be very significant and potentially may enable the material to deform without macroscopic brittle failure, thereby enhancing the fracture toughness of the composites [11]. However, such competing effects of glass fibres on the mechanisms of deformation and fracture of glass-filled nylon 6,6 have not been systematically studied. Furthermore, changes in the microstructures of the matrix materials, such as spherulite size, morphology and crystallinity can also affect the deformation behaviour of the material and thus the fracture properties of the composites [12, 13]. Increases in crystallinity by annealing, for example, are known to affect the mechanical properties of a semi-crystalline polymer significantly [14–24]. The combined effects of the fibre–matrix interactions on the overall deformation and fracture behaviour of a composite due to changes in microstructures have yet to be fully investigated [10, 25].

The annealing effects on the mechanical properties of a semi-crystalline polymer have been studied by many investigators [14–24]. For example, in studying the annealing behaviour of polypropylene (PP), Schotland [21] has shown that a critical annealing temperature was found, where a drastic decrease in ductility was observed. In nylon 6,6, similar changes in

0022–2461

the ductility by annealing were also reported [16, 18] and were suggested by Bell and Dumbleton [19] to be a result of conversion from chain-folded crystals (form I material) to partially extended crystals (form II material). On examining the annealing behaviour of poly(ethylene terephthalate) (PET), Elenga *et al.* [20] have also suggested that the drastic loss in drawability during annealing resulted from a morphological change due to transesterification in the amorphous phase. Other mechanisms, such as reorganization and perfection of most defective crystals [21, 22] and reduction of tie-chain molecules during lamellar thickening upon annealing [23, 24], have also been suggested to explain the observed annealing effects on the deformation behaviour of the materials. In the case of nylon 6,6 composites, however, the annealing effects on the mechanical properties of nylon 6,6 can be further complicated by the presence of glass fibres [25, 26].

In this study the deformation and fracture behaviour of a glass fibre-reinforced nylon 6,6 was examined by varying the content of glass fibres and the annealing conditions. In Part I [27], the effects of glass fibres and annealing conditions on the microstructural and morphological aspects have been presented. In this paper, the mechanical behaviours of nylon 6,6 matrix composites will be addressed.

2. Experimental procedure

2.1. Materials

The materials studied were poly(hexamethylene adipamide), or nylon 6,6, reinforced by chopped E-glass fibres. Details of the materials and microstructure are provided in Part I [27]. Both tensile specimens (ASTM D638) and 6.35 mm thick bend bars were injection moulded. Seven loading levels of fibre reinforcement, unreinforced, 1, 5, 10, 20, 30 and 40 wt % of the matrix, respectively, were examined. In order to investigate the effects of glass-fibre length on the mechanical properties of nylon 6,6 composites, a separate batch of composites were also made by diluting the 40 wt % glass composite with nylon 6,6 by reextrusion, followed by injection moulding. Because fibre breakdown during injection moulding was very significant in the 40 wt % glass composite [27], the average fibre length in the diluted composites was expected to be smaller than in the non-diluted composites. Composite specimens with glass fibre levels of 10, 20, 25 and 30 wt % were made in the diluted batch. The average glass-fibre lengths of the diluted and non-diluted composites are listed in Table I. To avoid moisture and light degradation effects, after injection moulding the specimens were kept in sealed PE film inserted inside a hot-seamed aluminized paper until they were tested.

The degree of crystallinity of the materials studied was changed through annealing of the specimens at 150 °C for various times. Three sets of samples, the unreinforced, 10 and 30 wt % glass-filled composites, respectively, were used to investigate the effects of annealing on the mechanical properties of the nylon 6,6 composites. Details of the annealing process and crystallinity determination were discussed in Part I [27].

TABLE I

Glass fibre content (wt %)	Average fibre length (μm)	
	Non-diluted composite	Diluted composite
10	380.4	291.3
20	364.4	281.7
25	–	214.5
30	263.1	213.5
40	232.1	237.1

2.2. Mechanical properties

The tensile properties of the materials studied were examined by the procedure of ASTM D-638 using a computer-controlled Instron hydraulic testing machine. Five specimens of each glass-fibre loading level and four annealed tensile samples at each annealing time were tested. The displacement rate used for all tensile testing was 5 mm min^{-1}. All tests were carried out at room temperature upon removal of specimens from the specimen storage bags.

2.3. Fracture toughness

The plane-strain fracture toughness, K_{IC}, was determined using a three-point bend method [28] on pre-cracked 6.35 mm thick bend bars. Pre-cracks were introduced into the specimens by inserting a fresh razor blade into a machined notch. Three bend samples were tested for each glass-fibre content and for each annealing condition. All tests were carried out at a speed of 5 mm min^{-1} and at room temperature upon removal of specimens from their moisture-proof bags. The thickness requirement for valid true plane-strain fracture toughness, K_{IC}, was checked using the equation

$$B_{req} = 2.5\left(\frac{K_Q}{\sigma_y}\right)^2 \quad (1)$$

where K_Q is the apparent fracture toughness and σ_y is the yield stress. The thickness requirement of Equation 1 for K_{IC} was satisfied for all glass-filled composites, but was not satisfied for the case of unreinforced nylon 6,6 for which case $K_Q \neq K_{IC}$.

2.4. *In situ* fracture observation and fractography

To provide a mechanistic understanding of the fracture behaviour in nylon 6,6 composites, the deformation and fracture process ahead of crack tips were observed *in situ*, as was done recently [10], by using a buckled-plate fixture [29] under an optical microscope. The details of this experimental technique have been reported elsewhere [10].

Fracture surfaces of the materials studied were also examined by scanning electron microscopy (SEM) in a

Joel JSM5200 electron microscope after fracture of the specimens.

3. Results

3.1. Tensile properties

3.1.1. Unreinforced nylon 6,6

The stress–strain curve of the unreinforced nylon 6,6 is shown in Fig. 1. Note that, after yielding, two distinct plateau regions in the stress–strain curve were observed. The onset and propagation of necking appeared only from the start of the second plateau region. In the first plateau region, the material was deformed at a constant load higher than the load required for neck propagation, and the deformation accumulated almost half of the total strain.

Further studies using loading–unloading tests (see Fig. 2) indicated that the energy loss during unloading–reloading, E_{hys}, or the hysteresis, increased with increasing strain in the first plateau region. However, the hysteresis remained constant in the second plateau region after necking commenced. In Fig. 3, the hysteresis energy is plotted against the strain at unloading. As can be seen, the hysteresis increased significantly in the first plateau region and dropped to a constant value after the formation of necking.

After annealing, some work hardening was exhibited in the first plateau region giving rise to a maximum strength higher than the yield stress (see Fig. 4). The change in the yield stress, tensile strength and the stress for neck propagation, namely, the second plateau stress, as a function of annealing time is plotted in Fig. 5. As can be seen, annealing for only 1 h produced a significant drop in all stress levels. This is consistent with the fact that thermal residual stresses due to injection moulding were removed during the first hour of annealing. It is expected that the yield stress would be significantly lowered if the compressive residual stresses on the specimen surface were removed. The thermal residual stresses in the injection-moulded specimens were estimated using the parabolic law [30]

$$\sigma(z) = \frac{\alpha E \Delta T}{2(1-\nu)}\left(\frac{1}{3} - \frac{z^2}{z_0^2}\right) \quad (2)$$

where z is the distance from specimen centre and z_0 is the half specimen thickness. By using $\alpha = 81 \times 10^{-6}\,K^{-1}$, $E = 1829$ MPa, $\nu = 0.46$ and $\Delta T = 190$ K, the estimated residual stress is found to be -17.4 MPa on the specimen surface, which correlates well with the magnitude of the decrease in the stress levels observed.

Annealing for times greater than 1 h causes the yield stress and tensile strength to increase (see Fig. 5).

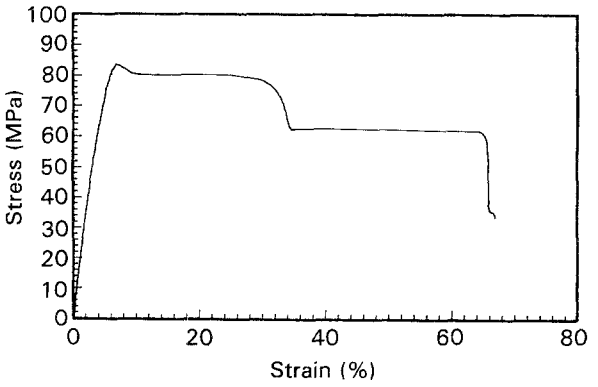

Figure 1 The nominal stress–strain curve for the unreinforced nylon 6,6.

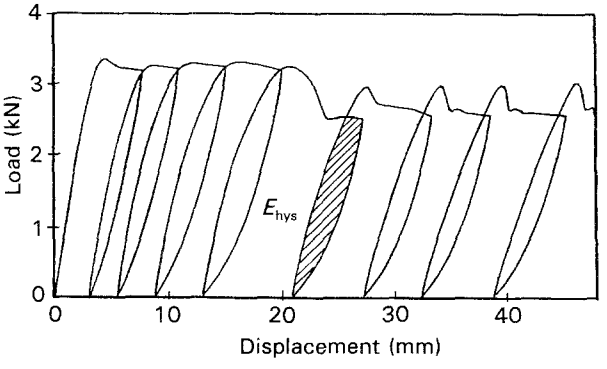

Figure 2 The load–displacement curve of the unreinforced nylon 6,6 showing the hysteresis in the plateau regions.

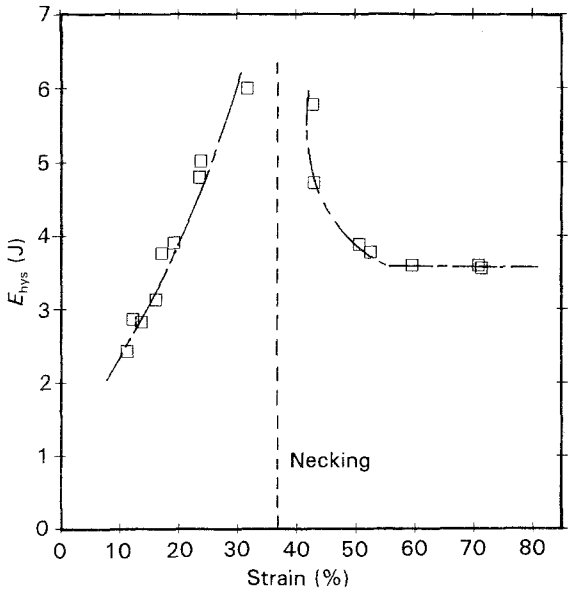

Figure 3 The energy loss of hysteresis versus corresponding strain at unloading for the unreinforced nylon 6,6.

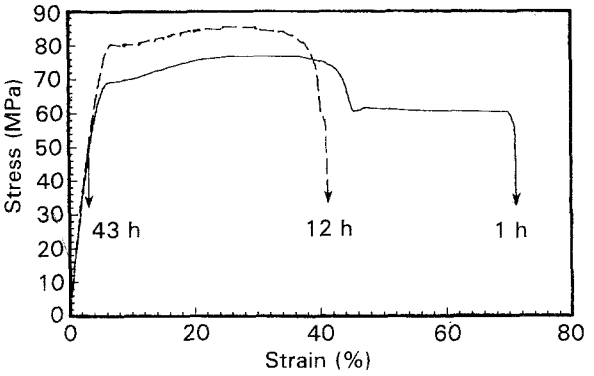

Figure 4 The stress–strain curves for the unreinforced nylon 6,6 annealed for 1, 12 and 43 h in vacuum.

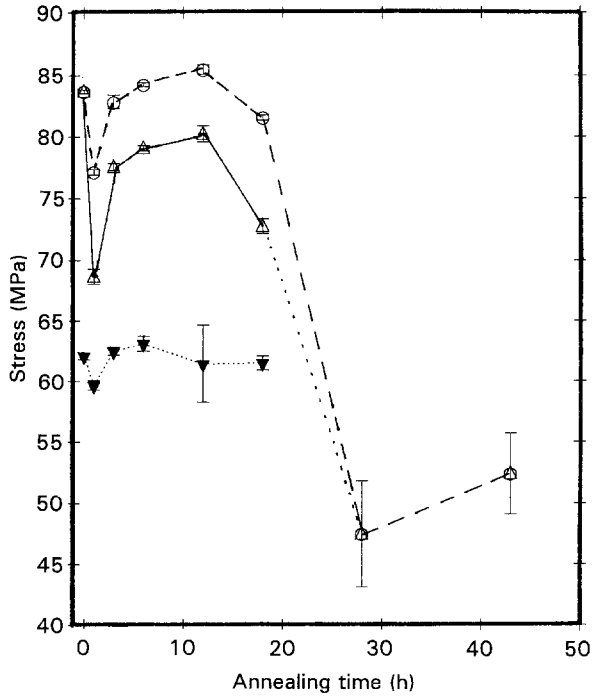

Figure 5 The annealing effects on the (△) yield stress, (○) tensile strength and (▼) the stress for neck propagation of unreinforced nylon 6,6.

Beyond 28 h annealing in vacuum, there was a sudden change from ductile post-yield to brittle pre-yield fracture of the tensile specimens, as represented by a sharp drop of the tensile strength in Fig. 5. Examination of the fracture surfaces of unannealed tensile specimens by SEM (Fig. 6) revealed ductile drawn fibrils of about 10 μm diameter. A closer look (see Fig. 6b) revealed the presence of interlinks between these drawn fibrils. On the other hand, the fracture surface of the tensile specimens annealed above the critical level showed a brittle fracture surface, as shown in Fig. 7. Upon closer examination, the brittle fracture surfaces (Fig. 7b) appeared to be transspherulitic. The transition from ductile to brittle fracture above a critical crystallinity by annealing (~ 40% in our case) has also been reported in other semi-crystalline polymers, such as PP [21], nylon 6 [18, 31] and PET [20].

In Fig. 8 the fracture strain, ε_f, yield strain, ε_y, and the strain at the onset of necking, ε_{neck}, are plotted as a function of annealing time. Note that the first hour of annealing produced an increase in the yield and fracture strain, which resulted from a removal of residual thermal stresses after annealing. The difference between the fracture strain and the strain at the onset of necking ($\varepsilon_f - \varepsilon_{neck}$), is the necking strain. Note from Fig. 8, that there was no significant necking strain beyond about 6 h annealing (~ 37% crystallinity). On the other hand, ($\varepsilon_{neck} - \varepsilon_y$) is the first plateau strain. It is evident from Fig. 8 that the onset of brittle behaviour represented a loss of strain equivalent to the first plateau strain ($\varepsilon_{neck} - \varepsilon_y$).

3.1.2. Nylon 6,6 composites

Fig. 9 shows the stress–strain curves for 1, 5, 10, 30 and 40 wt % glass fibre-reinforced nylon 6,6. As can be

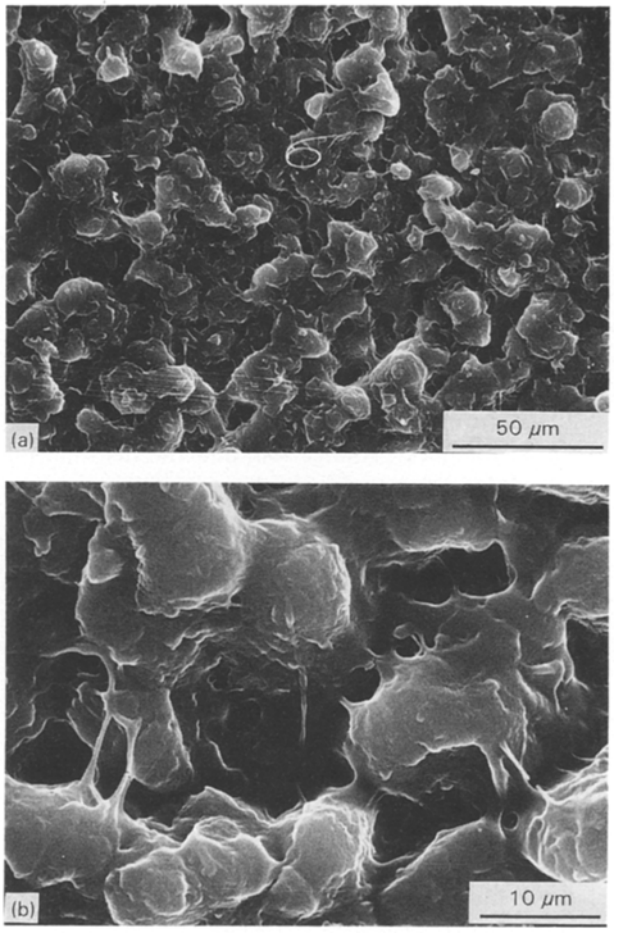

Figure 6 Scanning electron micrographs of the tensile fracture surface of unreinforced nylon 6,6 prior to annealing. (a) Low magnification, (b) higher magnification.

seen, the addition of small amounts of glass fibres caused the materials to fail at a relatively low strain, and the failure was in a brittle pre-yield manner. When the nylon 6,6 was reinforced by glass fibre contents greater than 30 wt %, yielding prior to fracture was observed. In Fig. 10 the tensile moduli of the composites are plotted as a function of glass-fibre content. The modulus prediction using the Haplin–Tsai equation [32] is also shown in Fig. 10. Note that the prediction of the Haplin–Tsai equation based upon discontinuous fibre reinforcement overestimates the modulus of composites with glass content greater than 20 wt %. This is consistent with the microstructural observation in Part I [27], namely that a significant reduction of glass fibre lengths was found in the composites with glass-fibre content greater than 20 wt %. Also note that in the case of diluted composites, which have a shorter average fibre length, the tensile moduli were lowered as compared to the non-diluted composites.

The composite yield stress and the strain at break versus glass-fibre content are shown in Fig. 11a and b, respectively. Note that the composites with glass contents ranging from 1–20 wt % were found to fail before macroscopic yielding occurs, resulting in a "dented" curve as shown in Fig. 11a. Similar results can also be found in the composite strain at break shown in Fig. 11b. The reappearance of macroscopic yielding

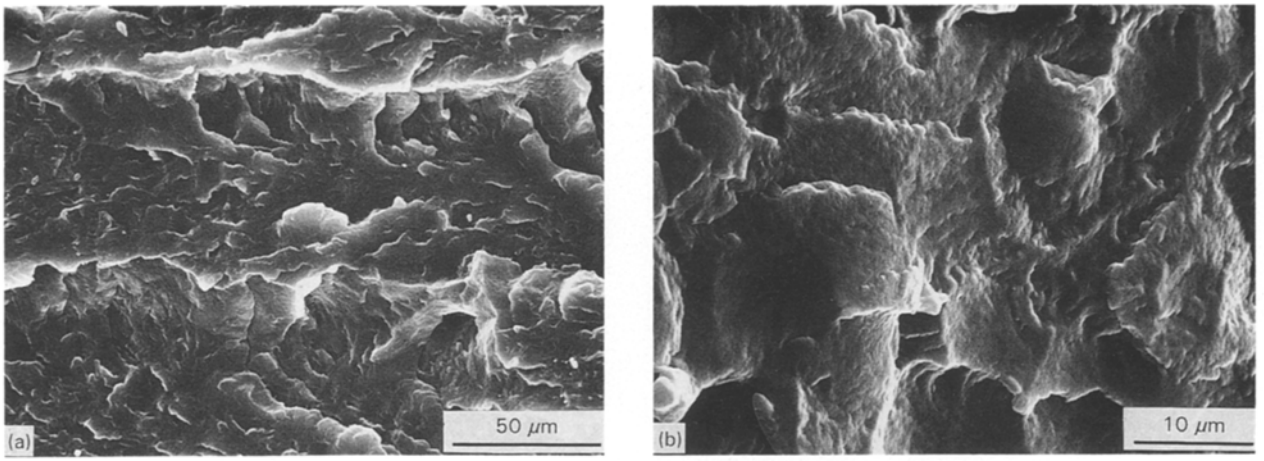

Figure 7 Scanning electron micrographs of the tensile fracture surface of unreinforced nylon 6,6 after 43 h annealing in vacuum. (a) Low magnification, (b) higher magnification.

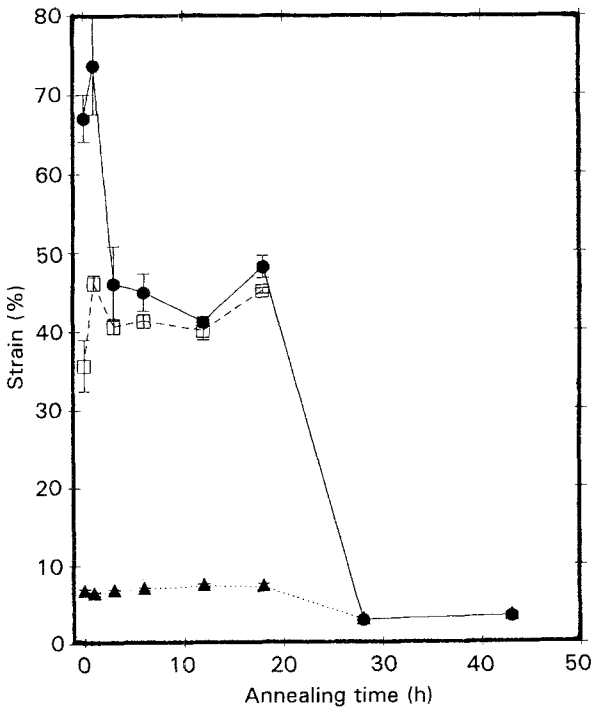

Figure 8 The annealing effects on the (●) fracture strain, (▲) yield strain and (□) the strain at the onset of necking in the unreinforced nylon 6,6.

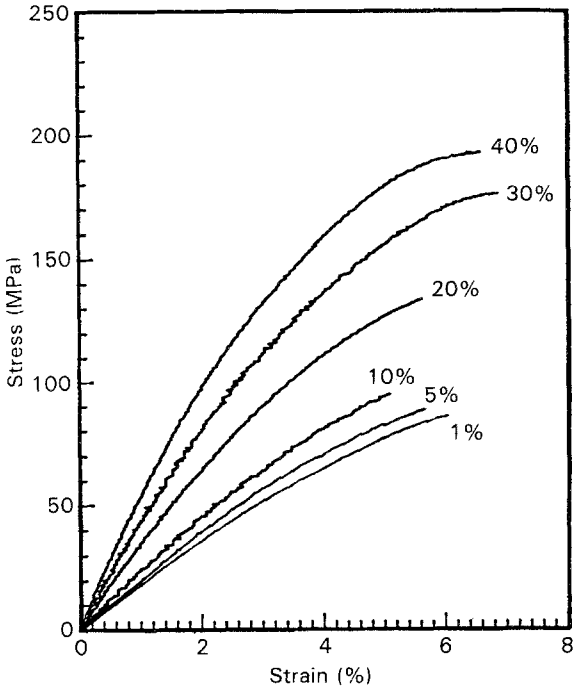

Figure 9 The effects of glass fibres on the nominal stress–strain curves of nylon 6,6 composite.

before sample failure was only seen in the composites with glass-fibre content greater than 30 wt %. In the diluted composites, the tensile strength was reduced (cf. Fig. 11a); however, ductilities were increased as compared to the non-diluted composites (cf. Fig. 11b). Furthermore, the transition from brittle pre-yield failure to ductile post-yield failure occurred at the smaller fibre content of 25 wt % compared to 30 wt % for the non-diluted composites.

Upon annealing, the tensile strength of the 30 wt % glass-filled composite were found to increase (see Fig. 12) while in the 10 wt % glass composite, a slight increase followed by a decrease in tensile strength was observed. In Fig. 13 the ductility of annealed 10 and 30 wt % glass-filled composites is plotted against the annealing time. Fig. 13 indicates a drop in ductility beyond a critical level of annealing. However, the magnitude of the drop in ductility, as well as the change of deformation mode observed in load–displacement curves, was not as significant as in the case of unreinforced nylon 6,6. The annealing effects on the tensile modulus, Fig. 14, were found to be only marginal for all the three sets of materials examined. Although one would expect an increase in elastic modulus by annealing due to an increase of crystallinity, the increases in the matrix crystallinity were limited in our case [27] and hence the change in elastic modulus by annealing was not significant.

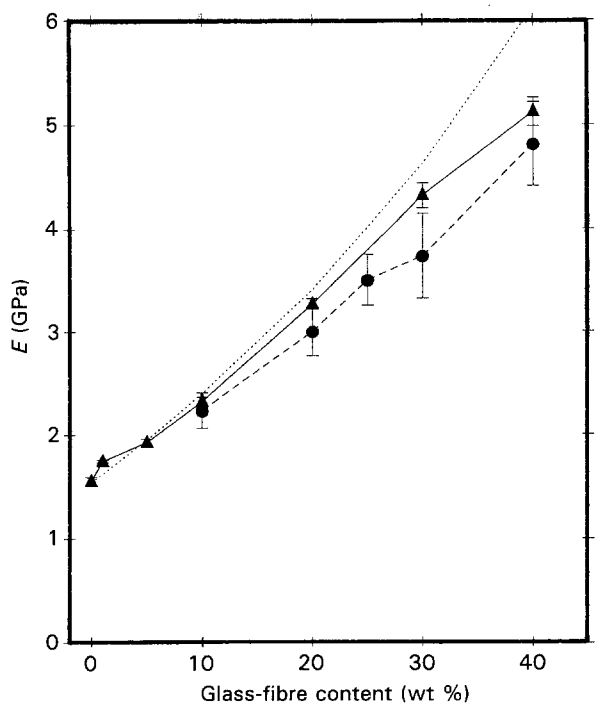

Figure 10 The effects of glass fibres on the tensile modulus of nylon 6,6 composites. (....) Halpin–Tsai equations. (▲) Non-diluted, (●) diluted composites.

3.2. Fracture toughness

The plane-strain fracture toughness, K_{IC}, as a function of glass-fibre content is shown in Fig. 15. Notice that the K_{IC} values of nylon 6,6 composites were lowered considerably by adding as little as 1 and 5 wt % glass fibres. Above about 10 wt % fibre content, the fracture toughness began to increase as the fibre content increased. However, as clearly seen from the "dented" K_{IC} curve shown in Fig. 15, only the specimens of the non-diluted batch with fibre content greater than 30 wt % showed a higher toughness value than that of their matrix material. Thus, as in the case of tensile properties, the transition to improved toughness of the composites is again associated with the glass fibre content of 30 wt %. In the case of diluted composites, however, the embrittlement effects due to the addition of glass fibres were found to be reduced and the composites showed much higher fracture toughness as compared to the non-diluted composites (see Fig. 15).

Mechanistic understanding of the embrittlement and toughening effects by glass fibres on the fracture toughness behaviour was provided by *in situ* fracture observations in front of a loaded crack tip. The results indicated that in the composites with low contents of fibre reinforcement, only a small amount of matrix plastic deformation was observed in the crack-tip region (see Fig. 16) and no fibre–matrix interfacial debonding could be observed prior to crack propagation. Fracture occurred by catastrophic propagation of the crack through linking up with the stress concentrated regions of fibre ends. Accordingly, little fibre bridging and fibre pull-out (see Fig. 17) occurred in the composites with low glass-fibre contents.

On the other hand, in the specimens containing more than 30 wt % glass fibres it was found that a

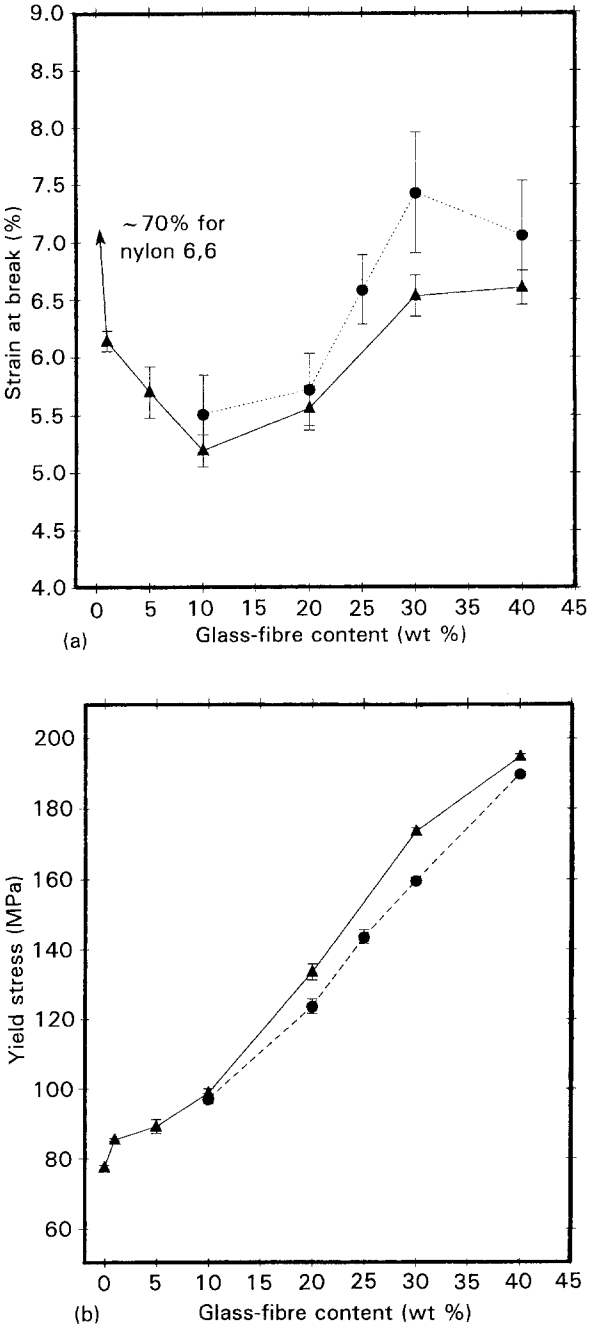

Figure 11 The effects of glass fibres on the tensile properties of glass-filled nylon 6,6: (a) fracture strain, and (b) yield stress versus glass-fibre content. (▲) Non-diluted, and (●) diluted composites.

greater degree of matrix plastic deformation occurred in the crack-tip region and at fibre ends, with the plastic zone size large enough to envelope fully several fibres (see Fig. 18). Similar results have also been noted by Sato *et al.* [8]. Limited stable crack growth due to crack bridging by unbroken fibres (see Fig. 18c) and a higher degree of fibre pull-out (see Fig. 19) were also observed. Such crack-wake toughening effects in the composites by glass fibres were not accounted for in the measurement of the K_{IC} values. The reported K_{IC} values are frontal zone toughness values. Attempts to characterize the R-curves of the composites were unsuccessful because of the relatively brittle nature of the materials.

In the diluted composites a somewhat larger plastic deformation zone, compared to the non-diluted case,

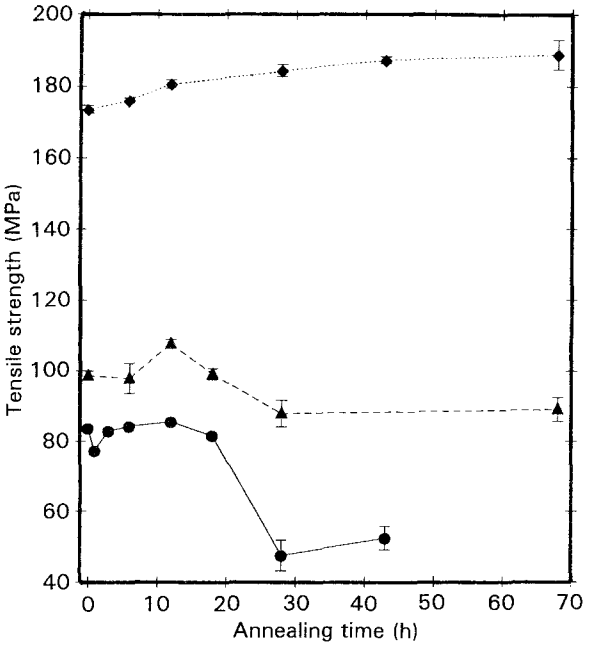

Figure 12 The annealing effects on the tensile strength of glass fibre-reinforced nylon 6,6. (▲) 10 wt %, (◆) 30 wt % glass composites, (●) unreinforced nylon 6,6.

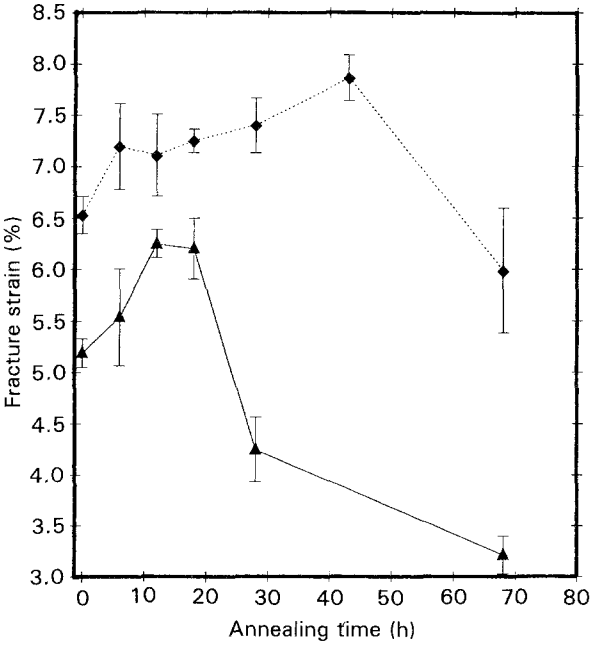

Figure 13 The annealing effects on the fracture strain of glass fibre-reinforced nylon 6,6. (▲) 10 wt %, (◆) 30 wt % glass composites.

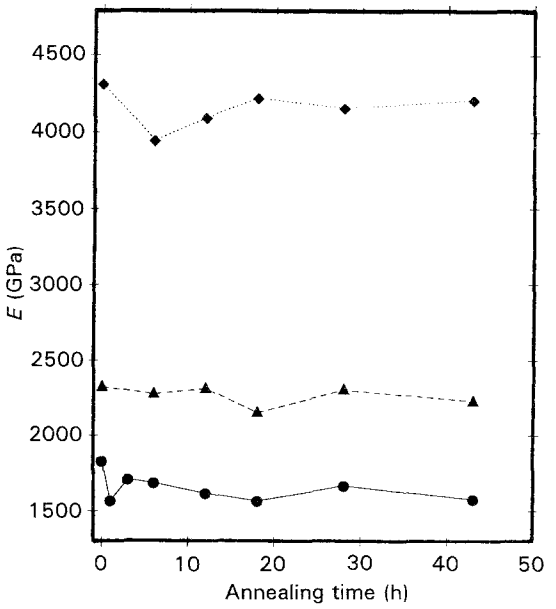

Figure 14 The annealing effects on the tensile modulus of (●) unreinforced, (▲) 10 and (◆) 30 wt % glass-filled composites.

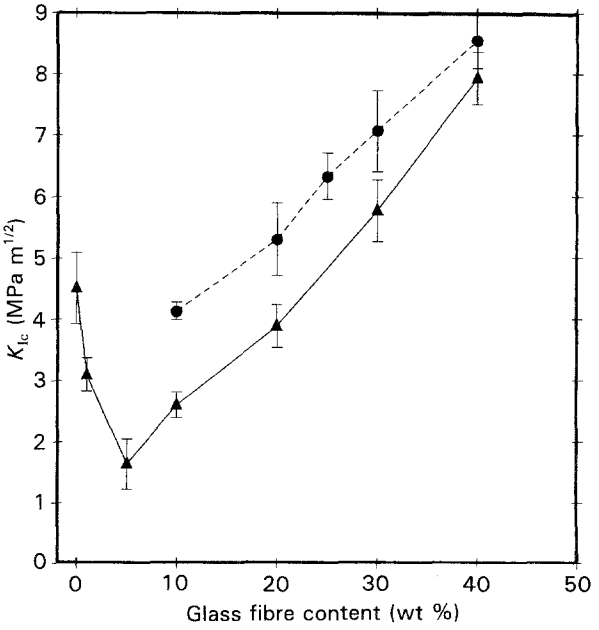

Figure 15 The effects of glass fibres on the fracture toughness, K_{IC}, of (▲) the glass fibre-reinforced nylon 6,6, and (●) diluted composites.

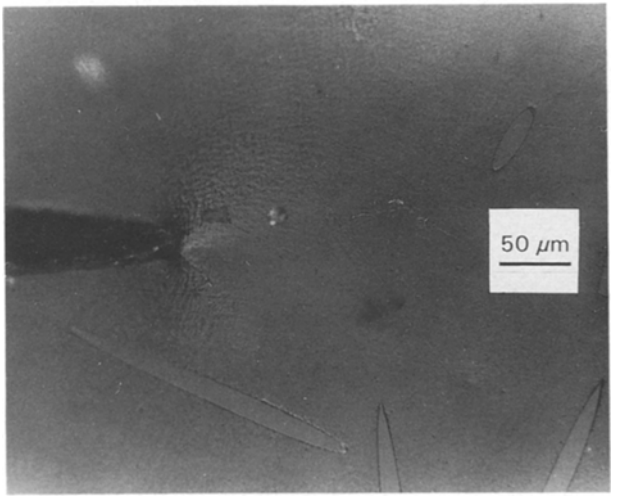

Figure 16 In situ fracture observation in front of a pre-crack shows limited crack-tip plasticity in 10 wt % glass-filled nylon 6,6.

was observed in the crack tip region, see Fig. 20a and b. Also, as can be seen in Fig. 20, the crack-tip opening prior to crack advance appeared to be larger in the diluted composites than in the non-diluted composites at the same value of the applied stress-intensity factor.

The observed fracture mechanisms in the glass fibre-reinforced nylon 6,6 during crack initiation, or the crack front stage, are summarized schematically in Fig. 21. As can be seen from the above results, together with the fracture toughness measurements, it is suggested that a critical glass-fibre volume fraction is

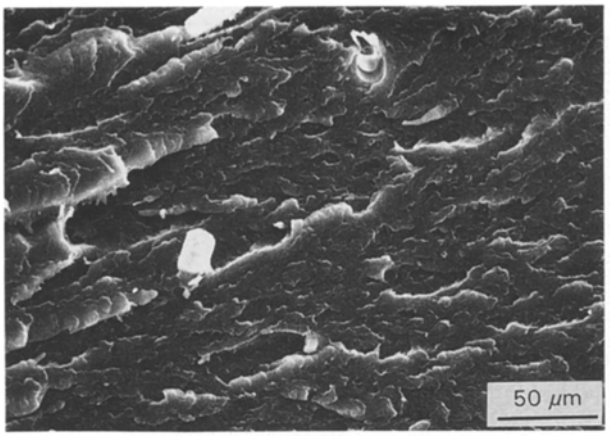

Figure 17 Scanning electron micrograph of the fracture surface in low glass-containing composite showing little fibre pull-out.

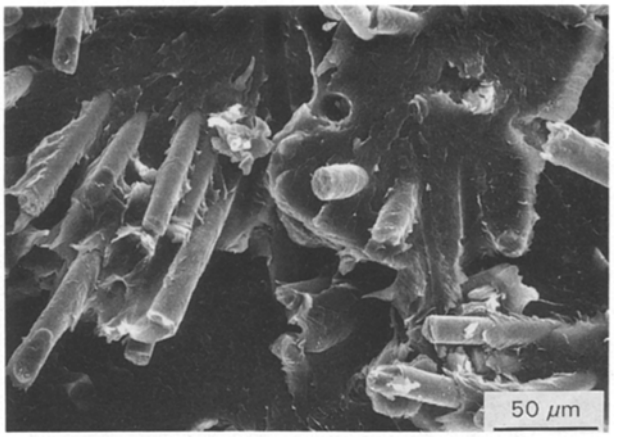

Figure 19 Scanning electron micrograph showing fibre pull-outs in the fracture surface of 30 wt % glass-filled composites.

needed in order to provide adequate matrix plasticity in the crack front so that failure occurs by ductile, rather than a brittle, failure mode. In our case, the critical glass-fibre content was found to be 30 wt % in the non-diluted composite specimens. Mechanisms in providing plasticity in the crack front will be further addressed in Section 4.

The annealing effects on the fracture toughness of both the unreinforced and glass fibre-reinforced nylon 6,6 are shown in Fig. 22. It should be noted, as mentioned, that in the case of unreinforced nylon 6,6 the toughness values measured were the apparent fracture toughness, K_Q, because the specimen thickness used was slightly smaller than the thickness required for true plane-strain fracture toughness (see Equation 1). As can be seen in Fig. 22, there was no significant change in the toughness for the unreinforced nylon 6,6 as the annealing time increases. This result was unexpected, because a transition from ductile post-yield fracture to brittle pre-yield fracture in tensile testing has been observed upon annealing above a critical level. This discrepancy will be discussed in Section 4.

In the case of composites shown in Fig. 22, the 30 wt % glass-filled composites showed a significant increase in the fracture toughness by annealing. In the 10 wt % glass-filled composites, the increase in toughness due to annealing was less significant.

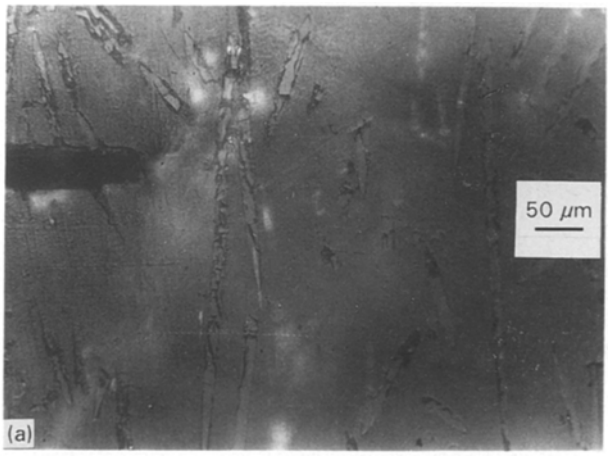

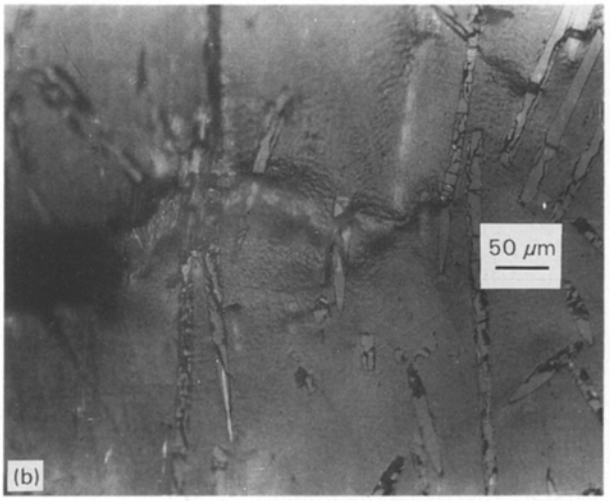

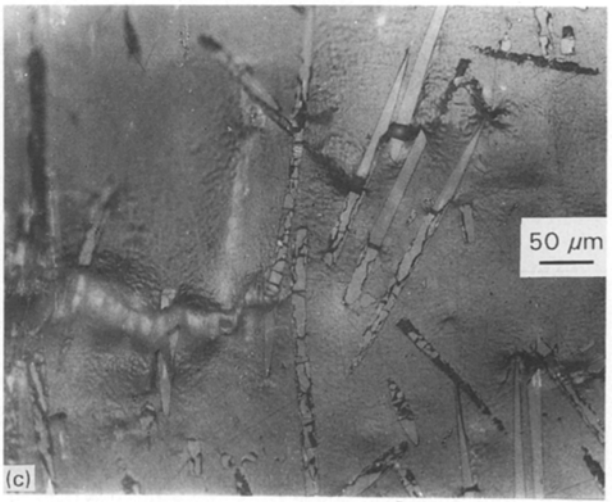

Figure 18 In situ fracture observations of 30 wt % glass composite showing (a) higher degree of matrix plasticity in the crack front, (b) formation of deformation zone by connecting the plasticity region at fibre ends, and (c) limited crack bridging by glass fibres in the crack wake.

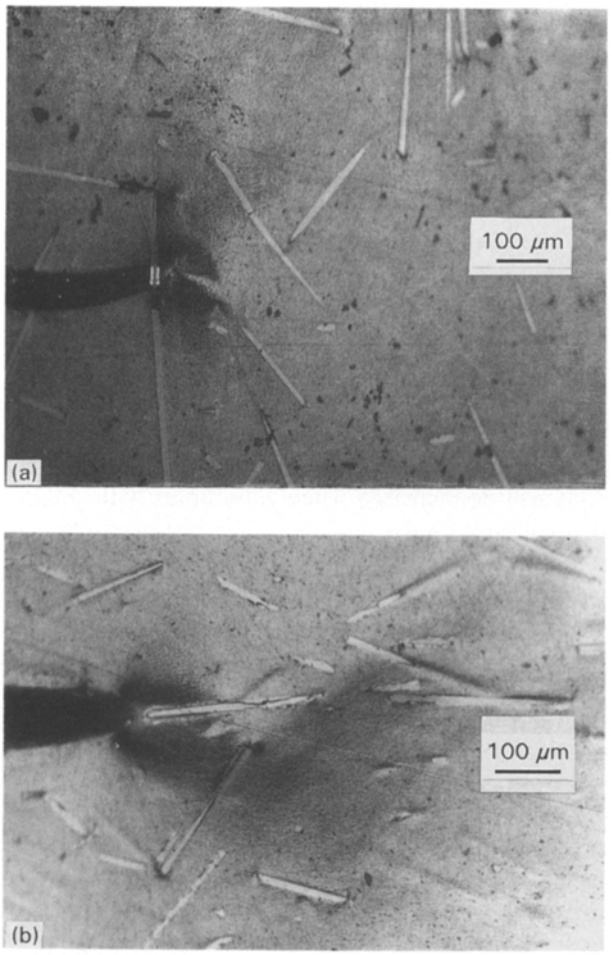

Figure 20 In situ fracture observations of plastic deformation zone at the same applied stress intensity: (a) 10 wt % non-diluted composite, (b) 10 wt % diluted composite.

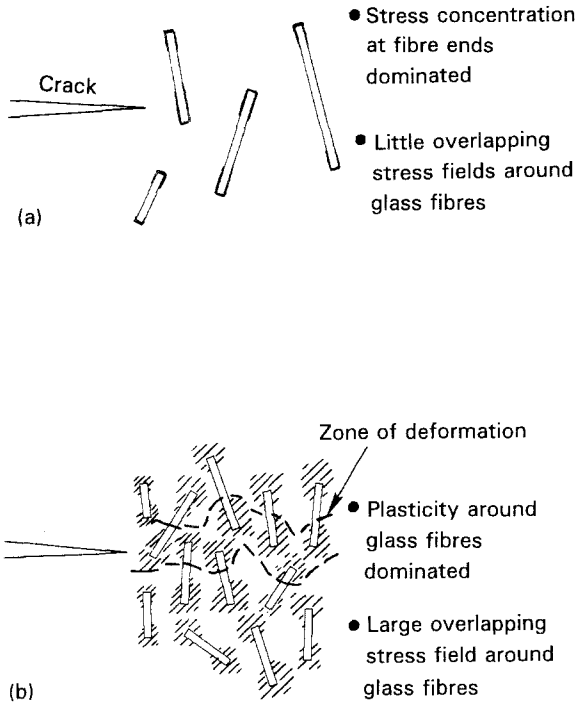

Figure 21 Schematic summary of the fracture mechanisms in the crack front of nylon 6,6 composites as observed by *in situ* fracture observations in (a) low glass-containing composites, and (b) high glass-containing composites.

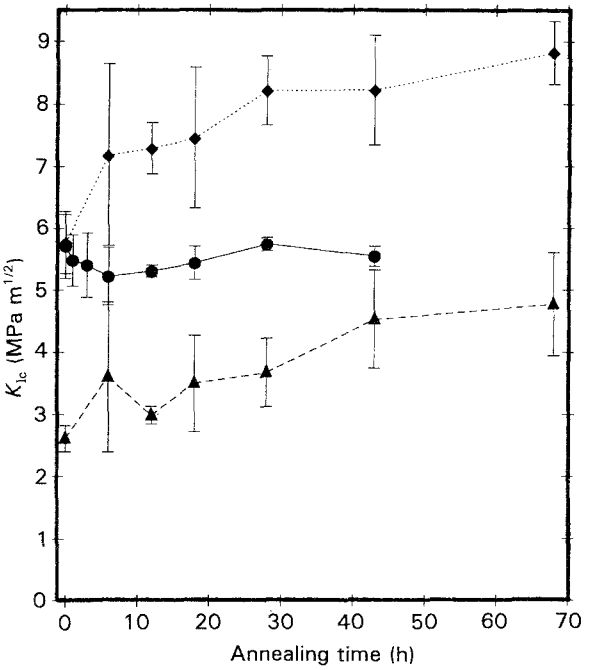

Figure 22 The annealing effects on the fracture toughness, K_{IC}, of nylon 6,6 with (▲) 10 wt %, (◆) 30 wt %, and (●) without glass-fibre reinforcements.

4. Discussion

4.1. Deformation behaviour of unfilled nylon 6,6

In the tensile stress–strain behaviour of unfilled nylon 6,6 it was found that two plateau regions exist in the stress–strain curves. Other results [33] in uniaxial tensile tests of nylon 6,6 also indicated the existence of two plateaus in the load–displacement curves, and an increase in the test speed tends to decrease the amount of deformation in the first plateau region. Similar stress–strain curves with two plateau regions have also been observed in other semi-crystalline polymers of poly(butylene terephthalate) (PBT) [34] and nylon 6 [35]. In semi-crystalline PBT, it has been found that the existence of the first plateau is related to a stress- or strain-induced phase transformation [36]. Previous studies on PBT [34] have shown that an increase in hysteresis with increasing strain in the first plateau is consistent with a deformation mechanism associated with a phase transformation. In such case, it was shown that [34]

$$E_{hys} \propto (\varepsilon - \varepsilon_y)^n \quad (3)$$

where E_{hys} is the hysteresis energy loss, ε_y is the yield strain and n was found to be about 0.5. Fig. 23 is a similar plot using the results from our study. As can be seen, a good fit to Equation 3 was observed with an n value of 0.51. These results may be viewed as an indication of a possible phase transformation upon loading, because in nylon 6,6 the conversion from form I material, represented by a higher-temperature endotherm, to form II material has been observed during cold drawing [19]. However, the total deformation strain accumulated in the first plateau was so large that it may not be fully accounted for by the transformation strains alone. Other deformation

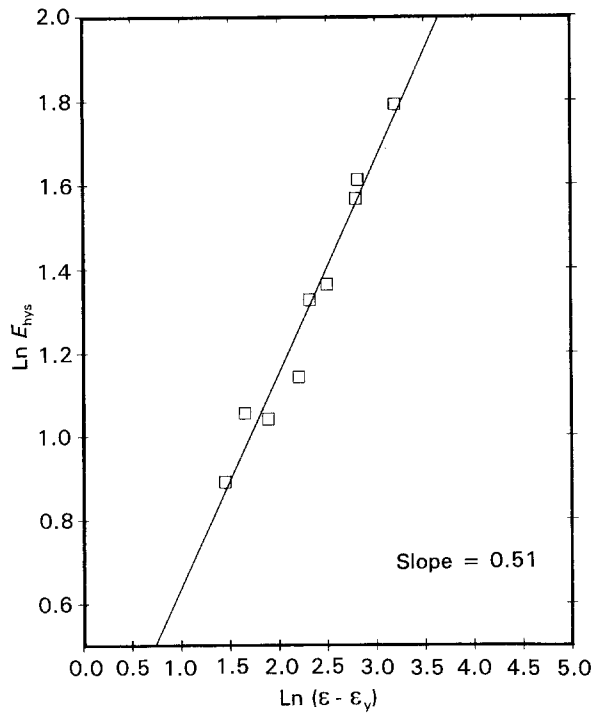

Figure 23 Log–log plot of hysteresis energy loss, E_{hys}, versus the strain at unloading in the first plateau region.

mechanisms, such as crazing in amorphous regions or viscous flow of amorphous regions, may also be considered as responsible for the deformation in the first plateau.

4.2. Glass-fibre effects

The effects of glass fibres on the mechanical properties of the composites were found to be strongly associated with the role of fibre ends. Microscopically, fibre ends are sites of the stress concentration which can enhance the propensity of crack propagation with relatively low fracture toughness. As a result, the fracture toughness of the composites can be significantly decreased by introducing only a small amount of glass fibres (see Fig. 15). The effects of stress concentration at fibre ends on the fracture toughness of the composites can be derived to be (see Appendix)

$$K_{cc} = \alpha\sigma^* f^{-1/6} \quad (4)$$

$$\alpha = (2\pi)^{1/2}\left(\frac{8}{\pi d_f^3 S}\right)^{-1/6} \quad (5)$$

where K_{cc} is the effective fracture toughness of the composite, f denotes the volume fraction of the glass fibres; d_f and S represent the diameter and aspect ratio of the glass fibre, respectively. Equation 4 is derived on the basis that failure ahead of cracks occurs when a critical stress, σ^*, is exceeded over some critical distance ahead of the crack tip. In this model, the critical distance is taken to be the spacing between fibre ends. The value of σ^* is considered as a constant independent of fibre volume fraction, because no interactions between fibre ends were assumed. An understanding of the magnitude of σ^* can provide mechanistic insights into the embrittlement effects of the fibre ends. The value of σ^* was obtained by fitting Equation 4 to the experimental data. Using the toughness data of 1 and 5 wt % glass composites, in which the materials failed predominantly by stress concentration effects, it is found that the value of σ^* in Equation 4 is approximately equal to the yield stress of the matrix, see Fig. 24. This result suggests that failure occurs when the first fibre end near the crack tip induces localized matrix yielding and subsequent void formation. Linkage of this void with the primary crack results in catastrophic failure. Note from Equation 4 that the toughness decrease due to an embrittlement effect is more sensitive to the fibre diameter than to the aspect ratio of the glass fibre, as can be seen in Fig. 24. The model predicts that the embrittlement effects at fibre ends will be increased when glass fibres with smaller diameter are used.

As the glass fibre content is increased, the plasticity at fibre ends can be significantly enhanced by overlapping stress fields of nearby glass fibres (see Fig. 21). Furthermore, as fibre ends approach each other with increasing fibre volume fraction, the plasticity at fibre ends begin to overlap, creating extensive plasticity around the crack tip, as was shown in Fig. 21. Failure is now ductile in nature and, as in ductile alloys, generally involves the linkage of several voids in an extended process zone around the crack tip. This can be illustrated by comparing the measured fracture toughness of the diluted and the non-diluted composites. As can be seen in Table I, the average fibre length in the diluted composites was much smaller than in the non-diluted composites, indicating a substantial increase of fibre-end density in the diluted composites. From Equation 4 one would thus predict a decrease in the fracture toughness of the composites when only the embrittlement effects of the fibre ends

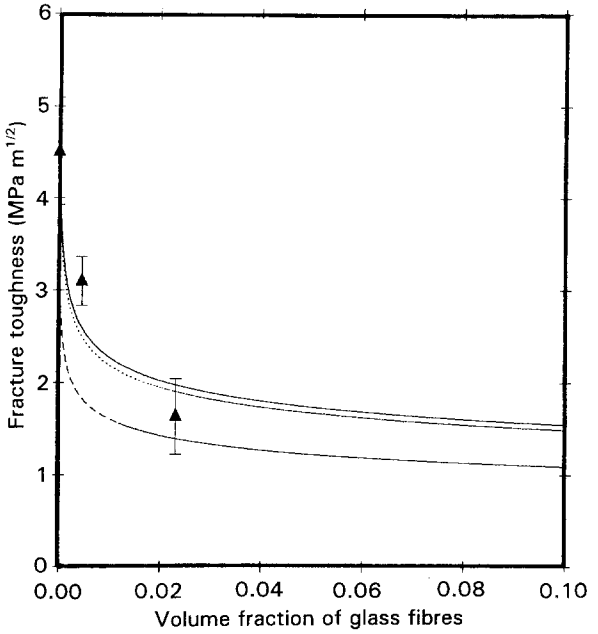

Figure 24 The effects of fibre-end stress concentration on the fracture toughness of the composite using Equation 4, with (——) d = 13 μm, S = 30, (– – –) d = 6.5 μm, S = 30, (- - -) d = 13 μm, S = 15. (▲) Experimental data.

were considered. On the contrary, the fracture toughness showed a substantial increase in the diluted composites as compared to the non-diluted composites (see Fig. 15). *In situ* fracture observations also showed that in the diluted composites a higher degree of crack-tip plasticity and larger crack opening prior to crack propagation were seen. This result strongly indicates that fibre-end plasticity can play an important role in the fracture behaviour of the composites.

Because the fibre-end plasticity can be increased by increasing fibre content, it is expected that a length parameter representing the size of a plastic deformation process zone must also be increased. It is known that the fracture energy directly scales with the size of the deformation process zone [11, 37]. However, the relationship for the process zone size due to interactions of fibre-end plasticity may not be readily obtainable. It is convenient to consider that the failure of the composite can occur when a critical strain, ε_f^*, is exceeded over a critical distance, l_c, from crack tip [38, 39]. This failure criterion results in a toughness equation of the form [38, 39]

$$K_{cc} = \left(\frac{\varepsilon_f^* \sigma_{yc} E_c l_c}{C_1 C_2} \right)^{1/2} \quad (6)$$

where σ_{yc}, E_c are the yield stress and tensile modulus of the glass composites, respectively, $C_1 \simeq 0.6$ and C_2 are constants. The value of C_2 may be determined from the Rice and Johnson [40] small-scale yielding solution of the distribution for plastic strain near the crack tip [39]. Using the tensile fracture strain of the composite, ε_{fc}, as the critical strain, ε_f^*, in Equation 6, the critical distance l_c can be obtained by fitting Equation 6 to the experimental data of K_{IC}. The results are shown in Fig. 25. As can be seen, the critical distance, l_c, for the 10 wt % ($\simeq$ 0.05% in volume) glass composite is only about one fibre-end spacing. As the glass content increases, the critical distance is also increased to about four fibre-end spacings in the 40 wt % ($\simeq$ 0.23% in volume) glass composite. This result suggests that the increase in fracture toughness due to fibre-end plasticity can be regarded as the increase of the critical distance, l_c. It is believed that such an increase in the critical distance, l_c, is directly related to the enhancement of the size of the deformation process zone. In the diluted composites shown in Fig. 25, the critical distance, l_c, appeared to be larger than in the non-diluted composites and was increased from about three to five times the fibre-end spacing as the glass-fibre content increases. Thus, the increase in fibre-end density in the diluted composite results in enhanced fibre-end plasticity, which in turn causes the observed increase in the fracture toughness of the composites.

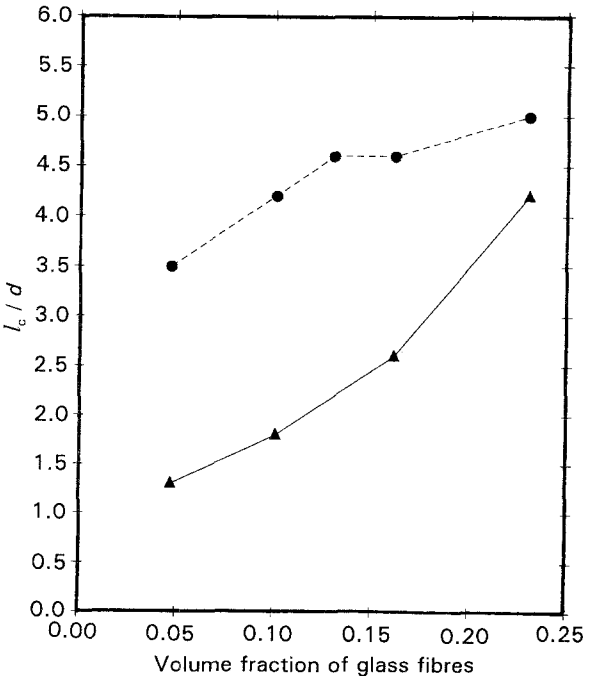

Figure 25 The calculated critical distance, l_c, versus glass fibre content for the (▲) non-diluted and (●) diluted nylon 6,6 composites.

Although fibre-end plasticity can contribute significantly to the fracture toughness of the composites, a critical amount of glass fibre is needed in order that substantial interactions of fibre ends can be generated to overcome the embrittlement effects of the fibre ends. The critical amount of glass fibre needed for toughness improvement depends on such factors as fibre type, fibre diameter and fibre–matrix interface properties. The effects of transcrystallinity due to glass fibres is expected to be negligible, as was discussed in Part I [27]. However, the change in spherulite size due to the addition of glass fibres cannot be neglected and will be discussed in Section 4.4. The effects of fibre diameter are now being investigated by the authors and will be published in a subsequent paper [41]. The change in matrix properties by annealing would inevitably affect the deformation behaviour around the glass fibres and hence the overall results of two competing mechanisms at fibre ends. The annealing effects will be discussed in the next section.

4.3. Annealing effects

In the unreinforced nylon 6,6 it was observed that a sharp drop of tensile properties can occur when the material was annealed above a critical level of annealing time (see Fig. 5). Similar results have also been reported in other semi-crystalline polymers including nylon polymers [16, 18, 31], PP [21] and PET [20]. In many cases, the change in tensile properties due to annealing has been correlated to the increase in crystallinity. In this study, the sharp drop in tensile ductility of annealed nylon 6,6 was also observed to occur when the crystallinity was increased above about 40% (28 h annealing), similar to the results obtained by other investigators [16, 18, 31]. However, it has been suggested that in low-temperature annealing, the melting and recrystallization of crystals are unlikely to occur and the crystals are often thickened with little change in crystallinity. Also, in studying the high-temperature annealing of PET, Elenga *et al.* [20] found that a drastic loss in drawability by annealing occurred at a nearly constant crystallinity. They suggested that such a change in drawability was caused by a morphology change from lamellar crystals to

fringed-micelle crystals during annealing. Hence, it is not clear that the change in tensile properties of annealed nylon 6,6 is solely due to the effects of increase in crystallinity, even though a critical crystallinity of about 40% has been observed in this study and by others [16, 18, 31]. In fact, it has been suggested that in nylon 6,6, a morphological change from lamellar crystals to fringed-micelle crystals during annealing is likely to occur due to its transamidation-prone nature [19, 20]. However, the exact mechanisms for explaining the observed change in tensile properties of annealed nylon 6,6 require further studies and thus only the correlations between tensile properties and annealing time are presented in this study.

In the case of fracture toughness measurements, however, such ductile–brittle transition behaviour upon annealing was not seen (see Fig. 22). This result was inconsistent with the tensile results, because the reduction of ductility and tensile strength is generally equivalent to a loss in the fracture toughness. In the uniaxial tensile test, the ductility reduction, as mentioned, was associated with a loss of the first plateau strain. However, in the presence of high triaxial stresses generated at the crack tip, it is possible that deformation mechanisms associated with the first plateau can still be operative even when the material is annealed above the critical level. The role of stress state on deformation mechanisms in the first plateau deserves further study.

In the glass-filled composites, annealing resulted in an increase in the fracture toughness (see Fig. 22). The magnitude of the toughness increase by annealing was more significant in the 30 wt % glass composite than in the 10 wt % glass composite, indicating that annealing had a much stronger influence in the ductile region of composite failure. Such a significant increase in the fracture toughness by annealing may be related to the changes in the matrix microstructure (see below) and the removal of residual stresses within the composites. Owing to the annealing effects, it appeared that the curve of fracture toughness versus the glass-fibre content shown in Fig. 15 shifted in a counterclockwise fashion by annealing, as schematically shown in Fig. 26. As a result, the critical glass-fibre content is decreased by annealing.

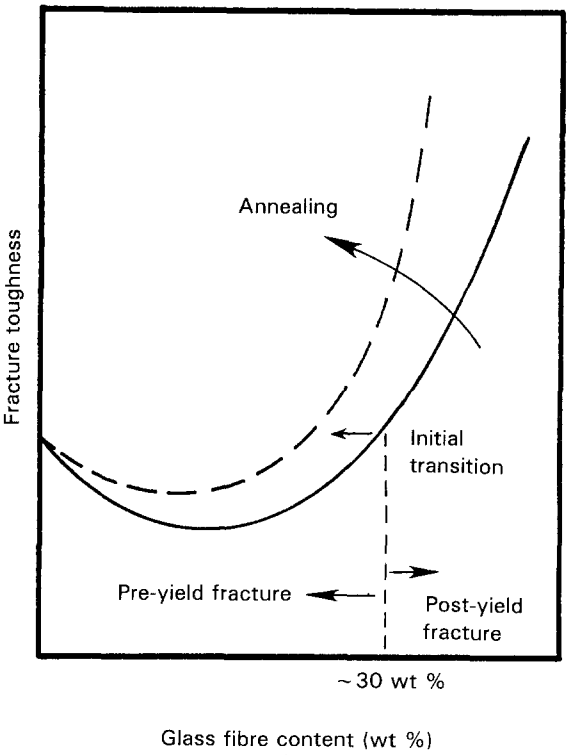

Figure 26 Schematic illustration of the combined effects of glass fibres and annealing on the fracture toughness, K_{IC}, in glass fibre-reinforced nylon 6,6.

4.4. Morphology effects

In Part I [27], it was shown that the spherulite size of nylon 6,6 can be decreased by the addition of glass fibres. Such a decrease in spherulite size is most likely a result of the excess crystal nuclei remaining in the polymer melt during injection moulding [27]. Changes of spherulite size in a semi-crystalline polymer are known to affect the material's yield strength and ductility [12]. However, the roles of spherulite size in the observed property changes have not been fully established because, in many cases, changes in crystallite dimensions were generally associated with variations in spherulite size [12]. Nevertheless, studies of the spherulite size refinement by nucleation agents [42] have indicated an improved ductility and yield strength. Similar effects on the composite's properties would thus be anticipated, provided that the embrittlement effects due to glass fibres could be excluded. Hence, in the composites with low glass-fibre content, the size of spherulite is believed to be only secondary with respect to the effects of glass fibres. In the composites with high glass-fibre content, which generally showed a macroscopic yielding, the spherulite size effects may be more significant. However, other changes in physical structures of the lamellae by changing the spherulite size can also be important. A decrease in crystallinity and possibly a smaller crystal thickness [12], for example, can occur and may allow a greater margin of property improvements through annealing. For instance, the significant increase in the fracture toughness of nylon 6,6 composites by annealing may be related to this effect.

4.5. Property optimization

The above results lead to the question of competing roles of glass fibres in optimizing the mechanical properties of a short-fibre-reinforced polymer composite. Longer fibre length is known to improve significantly the tensile strength and modulus of the composites; however, such improvement may be limited by the embrittlement effect at fibre ends (see Equation 4) and result in a brittle fracture of the composites. On the other hand, an increase in fibre-end density can provide enhanced localized matrix plasticity and thereby enhance the fracture toughness of the composites. Such an increase in fracture toughness may be achieved by increasing the fibre-end density through increasing the amount of glass fibres. However, the increase in glass-fibre content would inevitably cause more severe fibre breakdown during

injection moulding and result in a shorter glass-fibre length. Consequently, the enhancement in tensile strength and modulus would be limited. The use of glass fibres with smaller diameter, which can provide both higher fibre strength and higher interfacial shear stresses to generate matrix plastic deformation, may provide better property improvements in the composites. On the other hand, the embrittlement effects at fibre ends would also increase in parallel to the decrease of the fibre diameter. As a result, the competing roles of glass fibres may still be present. The effects of a small-diameter fibre on mechanical properties of nylon 6,6 have been studied by Sato *et al.* [43] and by Watkins *et al.* [44]. Improved mechanical properties have been observed for composites with smaller fibre diameter and the existence of an optimum fibre diameter has also been suggested [43]. However, the role of fibre diameter on the fundamental aspects of the competing roles of glass fibres on deformation and fracture behaviour needs further study.

5. Conclusions

1. In the unreinforced nylon 6,6, a region of non-necking deformation under a constant load was observed. It is suggested that such deformation is due, in part, to a stress-/strain-induced phase transformation.

2. In the nylon 6,6 glass composites, below a critical amount of approximately 30 wt % glass fibres, failure was pre-yield brittle. Above 30 wt %, fracture was post-yield ductile. The existence of the critical level of glass fibre content was explained based on the ductilization effect of localized plasticity at fibre ends.

3. *In situ* fracture observations indicated that in the low glass-content composites only very limited crack-tip plasticity can be seen. Failure was dominated by stress concentration effects at fibre ends. In the composites with glass-fibre content greater than 30 wt %, however, significant fibre-end plasticity was observed. Increasing fibre end density tends to increase the fibre-end plasticity by the overlapping of stress fields associated with nearby fibre ends.

4. The addition of a small amount of glass fibres caused a sharp decrease in the fracture toughness of the composites according to a $-1/6$ power of the glass fibre volume fraction. The fracture toughness showed an increase when the glass fibre content was higher than 10 wt %. The increase in the fracture toughness by glass fibre content was related to an increase in the size of deformation process zone due to enhanced fibre-end plasticity.

5. Annealing above a critical level caused a sharp change in strength and ductility of the unreinforced nylon 6,6. The changes in the tensile properties above the critical level were less significant in the glass composites. It was found that the fracture toughness of the composites can be significantly improved by proper annealing.

Acknowledgements

This work was supported by a grant from the Monsanto Chemical Company, Springfield, MA. Helpful discussions with Dr Robert L. Kruse, Monsanto Chemical Company, are also gratefully acknowledged.

References

1. M. F. ASHBY, *Acta Metall.* **37** (1989) 1273.
2. T. VU-KHANH, *Polym. Compos.* **8** (1987) 363.
3. P. K. MALLICK, "Fiber-reinforced Composites: Materials, Manufacturing and Design" (Marcel Dekker, New York, 1988) p. 1.
4. D. W. CLEGG and A. A. COLLYER (eds), "Mechanical Properties of Reinforced Thermoplastics" (Applied Science, New York, 1986).
5. W. V. TOTOW and B. J. LANHAM, "Reinforced Thermoplastics" (Applied Science, London, 1975) p. 1.
6. M. J. FOLKES, "Short Fiber Reinforced Thermoplastics" (Research Studies Press, Chichester, 1982) p. 31.
7. P. T. CURTIS, M. G. BADER and J. E. BAILEY, *J. Mater. Sci.* **13** (1978) 377.
8. N. SATO, T. KURAUCHI, S. SATO and O. KAMIGAITO, *ibid.* **26** (1991) 3891.
9. K. TAKAHASHI and N. S. CHOI, *ibid.* **26** (1991) 4648.
10. S. V. NAIR, M. L. SHIAO and P. D. GARRETT, *ibid.* **27** (1992) 1085.
11. B. LAUKE, B. SCHULTRICH and W. POMPE, *Polym. Plast. Technol. Eng.* **29** (1990) 607.
12. J. M. SCHULTZ, *Polym. Eng. Sci.* **24** (1984) 770.
13. A. J. KINLOCH and R. J. YOUNG, "Fracture Behavior of Polymers" (Applied Science, London, 1983) Ch. 9.
14. A. PETERLIN, *J. Appl. Phys.* **35** (1964) 75.
15. E. W. FISHER, *Pure Appl. Chem.* **31** (1972) 113.
16. H. W. STARKWEATHER Jr, G. E. MOORE, J. E. HANSEN, T. M. RODER and R. E. BROOKS, *J. Polym. Sci.* **XXI** (1956) 189.
17. G. C. ALFONSO, E. PEDEMONTE and C. PONZETTI, *Polymer* **20** (1979) 104.
18. D. P. RUSSELL and P. W. R. BEAUMONT, *J. Mater. Sci.* **15** (1980) 216.
19. J. P. BELL and J. H. DUMBLETON, *J. Polym. Sci. A-2* 7 (1969) 1033.
20. R. ELENGA, R. SEGUELA and F. RIETSCH, *Polymer* **32** (1991) 1975.
21. R. S. SCHOTLAND, *Polym. Eng. Sci.* **6** (1966) 244.
22. B. WUNDERLICH, "Macromolecular Physics", Vol. 3 (Academic Press, New York, 1980) Ch. 9.
23. M. J. McCREADY and J. M. SCHULTZ, *J. Polym. Sci. Polym. Phys.* **17** (1979) 725.
24. S. NAGOU and S. OBA, *J. Macromol. Sci. Phys.* **B18** (1980) 281.
25. G. P. DESIO and L. REBENFELD, *J. Appl. Polym. Sci.* **39** (1990) 825.
26. T. BESSELL and J. B. SHORTFALL, *J. Mater. Sci.* **10** (1975) 2035.
27. M. L. SHIAO, S. V. NAIR, P. D. GARRETT and R. E. POLLARD, *ibid.* **29** (1994) ▮.
28. "Protocal on Plain-Strain Fracture Toughness and Strain Energy Release Rate of Plastic Materials", ASTM Subcommittee D20.10.21 (American Society for Testing and Materials, Philadelphia, PA, 1989).
29. P. CHANG and J. A. DONOVAN, *J. Mater. Sci.* **24** (1989) 816.
30. B. D. AGGARWALA and E. SAIBEL, *Phys. Chem. Glasses* **2** (1961) 137.
31. T. J. BESSELL, D. HULL and J. B. SHORTFALL, *J. Mater. Sci.* **10** (1975) 1127.
32. J. C. HAPLIN and J. L. KARDOS, *Polym. Eng. Sci.* **16** (1976) 344.
33. M. I. KOHAN (ed.), "Nylon Plastics" (Wiley, New York, 1973) p. 333.
34. P. CHANG, PhD thesis, University of Massachusetts, Amherst (1992).
35. Y. LIU and J. A. DONOVAN, private communication (1992).
36. E. DOBROVOLNY-MARAND, PhD thesis, University of Massachusetts, Amherst (1987).

37. B. BUDIANSKY, J. W. HUTCHINSON and J. C. LAMBROPOULOS, *Int. J. Solids Struct.* **19** (1983) 337.
38. R. K. PANDEY and S. BANERJEE, *Int. Fract. Mech.* **10** (1978) 817.
39. R. O. RITCHIE, W. L. SERVER and R. A. WULLAERT, *Metall. Trans.* **10A** (1979) 1557.
40. J. R. RICE and M. A. JOHNSON, "Inelastic Behavior of Solids", edited by M. F. Kanninen, W. F. Adler, A. R. Rosenfield and R. I. Jaffee, (McGraw Hill, New York, 1970) p. 641.
41. S. V. NAIR and M. L. SHIAO, to be published.
42. F. J. PADDEN and H. D. KEITH, *J. Appl. Phys.* **30** (1959) 1479.
43. N. SATO, T. KURAUCHI, S. SATO and O. KAMIGAITO, *J. Compos. Mater.* **22** (1988) 850.
44. J. C. WATKINS, P. C. GAA and R. G. SWISHER, in "Proceedings of the ANTEC '88", Atlanta, April 1988 (Society of Plastic Engineers, Brookfield, CT, 1988) p. 528.

Received 27 August 1992
and accepted 27 September 1993

Appendix. A fracture toughness model for brittle composite failure associated with fibre ends

Consider a simple composite model of an isolated glass fibre with its fibre ends located at a distance, d, from the crack tip, as shown in Fig. A1. Assume that the material is free from any residual stresses and is uniformly loaded by a remote applied stress. Assuming that failure occurs when a characteristic stress σ^*, is exceeded over the distance, d

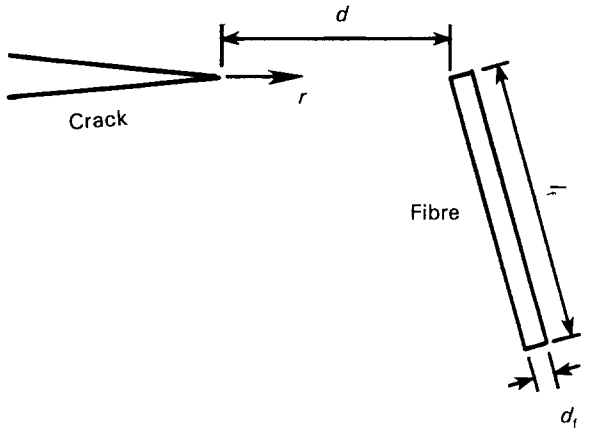

Figure A1 A glass fibre end located a distance, d, from the crack tip.

$$\sigma(r = d) = \sigma^* = \frac{K_{cc}}{(2\pi d)^{1/2}} \quad \text{(A1)}$$

or

$$K_{cc} = \sigma^*(2\pi d)^{1/2} \quad \text{(A2)}$$

where K_{cc} is the critical stress intensity factor of the composite. The distance, d, can be regarded as the average distance between fibre ends and hence can be related to the fibre-end density, ϕ, by

$$\frac{1}{d^3} = \phi = \frac{2f}{V_f} \quad \text{(A3)}$$

where f denotes the volume fraction of glass fibres and V_f is the volume of a single glass fibre. V_f can be written as

$$V_f = \frac{\pi}{4} d_f^2 l_f = \frac{\pi}{4} d_f^3 S \quad \text{(A4)}$$

where d_f, l_f is the diameter and the length of the glass fibre, respectively, and S represents the aspect ratio of the fibre. Introducing Equation A4 into Equation A3 and rearranging, we have

$$d = \left(\frac{8f}{\pi d_f^3 S}\right)^{-1/3} \quad \text{(A5)}$$

Thus the critical stress intensity factor or the plane-strain fracture toughness of the composite, K_{cc}, from Equation A2, becomes

$$K_{cc} = \alpha\sigma^* f^{-1/6} \quad \text{(A6)}$$

$$\alpha = (2\pi)^{1/2}\left(\frac{8}{\pi d_f^3 S}\right)^{-1/6} \quad \text{(A7)}$$